In-situ monitoring techniques for membrane fouling and local filtration characteristics in hollow fiber membrane processes: a critical review

Xianhui Li[a,c], Yinghiu Mo[a], Jianxin Li[a,b*], Wenshan Guo[d], Huu Hao Ngo[d]

[a]State Key Laboratory of Separation Membranes and Membrane Processes, School of Materials Science and Technology, Tianjin Polytechnic University, Tianjin 300387, P. R. China

[b]School of Environmental and Chemical Engineering, Tianjin Polytechnic University, Tianjin 300387, P. R. China

[c]Rabin Desalination Laboratory, Grand Water Research Institute, Wolfson Faculty of Chemical Engineering, Technion-Israel Institute of Technology, Haifa 32000, Israel

[d]Center for Technology in Water and Wastewater, School of Civil and Environmental Engineering, University of Technology Sydney, Sydney, NSW 2007, Australia

[*]Corresponding Author. jxli@tjpu.edu.cn

Abstract

Membrane fouling is the most serious challenge in the hollow fiber microfiltration (MF) and ultrafiltration (UF) processes. A number of in-situ monitoring techniques including optical and non-optical probes have been developed so that membrane fouling is better understood and controlled. This will help advance the membrane technology. In addition, the local filtration hydrodynamics wield a great influence on the membrane fouling formation and system operation stability. State-of-the-art in-situ monitoring techniques for membrane fouling and local filtration characteristics in hollow fiber MF/UF processes are critically reviewed. The principles and applications of these techniques are addressed in order to assess

their strengths. This study demonstrated that the real-time observation techniques mainly focus on idealized laboratory apparatus and little on commercial membrane modules. Consequently, more attention should be paid to the development of simple and effective methods or integrated detecting technology so as to satisfy the real status of hollow fiber filtration processes and the optimization of membrane module. On the basis of this review, future analyses considering practical requirements are suggested as R&D priorities.

Keywords: In-situ monitoring techniques; Hollow fiber membrane; Micro- and ultra-filtration processes; Membrane fouling; Filtration hydrodynamics

Nomenclature

c	velocity of the sound beam, m/s
c_b	local bulk protein concentration, kg/m^3
c_{bi}	local bulk protein concentration at the hemofilter's inlet/outlet, kg/m^3
dS	thickness of fouling layer, m
dt	difference in arrival time between fouling layer and membrane echo signals, s
f_D	Doppler shift, Hz
f_r	frequency transmitted by the transducer, Hz
J_i	local permeate flux, m/s
N	number of fibers
Q	permeate flow, m^3/s
Q_i	inlet flow, m^3/s

R_i fiber inner radius, m

v_s sound velocity in fouling layer, m/s

V blood flow velocity, m/s

Greek Letters

γ radioactivity of the radiolabeled marker, Bq

θ angle of the insonation

1. Introduction

As a preferable configuration for industrial applications, hollow-fiber membrane modules are now widely used not only in water treatment but also the biomedical field due to the larger membrane area per unit volume and enhanced productivity [1-3]. These advantages are ascribed to the characteristics of hollow fiber membrane module, which consists of a large number of fine membrane fibers straightly packed in module shell housing, and not requiring spacers between the membranes. Generally, the hollow fiber membrane module can be divided into the pressurized membrane module and submerged membrane module based on the filtration mode. Besides, the submerged hollow fiber membrane module could be oriented vertically and horizontally in practical applications.

Recently, to satisfy increasing engineering demands, the size of commercial hollow fiber membrane module has increased by up to 30 cm in diameter and 2.5 m in length [4-5]. Simultaneously, many thousands of hollow fiber membrane modules are installed together in

one plant. This will lead to a great challenge in terms of managing the technological risk since the local hydrodynamic conditions in the membrane module become more complex and non-uniform with the increase of module size. Furthermore, it will aggravate membrane fouling and system operating instability. These limitations can reduce productivity, increase energy consumption and shorten the membrane's lifespan. Thus, the membrane fouling and complex hydrodynamics are major challenges that can hinder the large-scale application of hollow fiber membrane filtration systems [6-7]. It is very important to obtain a better understanding of the relationship between the membrane fouling and filtration behavior of hollow fiber membrane, in order to provide new insights into the membrane fouling control.

To better understand the basic membrane fouling phenomena, the most effective strategy is the development and utilization of a suitable in-situ and non-invasive technique to obtain relevant and useful information about the foulant deposition process, deposit structure or distribution along the fiber [8-11]. However, not all non-invasive techniques are suitable to in-situ monitoring of hollow fiber membrane fouling. The reason is that the fine hollow fiber membranes consist of specific structures of small diameter and multiple curved surfaces, making it much harder to monitor membrane fouling deposition and hydrodynamic behavior in the hollow fiber membrane module. For the hollow fiber configuration, an internal pressure drop is caused by fluid flow in the fiber lumen, resulting in a decrease in trans-membrane pressure (TMP) along the fiber [12]. Accordingly, this non-uniform local flux distribution will lead to the aggravation of membrane fouling and uncertainty about operational matters. Specifically, the instability of local filtration behavior will intensify with the increase of the membrane module size. Thus, the design and optimization of the

membrane module have received much more attention during practical applications. There is considerable evidence that properly designed membrane modules can dramatically improve the fluid hydrodynamic conditions and enhance overall system performance [13-14]. Numerous attempts have been conducted to investigate the filtration behavior of hollow fiber membrane via experimental methods [15-17]. However, there are very few comprehensive reviews concerning local permeate properties of hollow fiber membrane, especially the relationship between local membrane fouling and filtration behavior.

This review is organized in four sequential sections: (1) in-situ monitoring techniques for hollow fiber membrane fouling, (2) in-situ monitoring methods for local filtration characteristics, (3) Future R&D direction and (4) concluding remarks. It also intends to illustrate the appropriate monitoring methods of local membrane fouling and filtration properties, and provide new insights into the module design for practical applications.

2. In-situ monitoring techniques for membrane fouling

Generally, the morphology and chemical constituents of foulants deposited on the hollow fiber membrane surface can be characterized using SEM (Scanning Electron Microscopy), EDX (Energy Dispersive X-ray), FTIR (Fourier Transform Infrared) or CLSM (Confocal Laser Scanning Microscopy), etc. [18-21]. These destructive measuring methods provide important information on the properties of fouling deposition on the membrane surface and within the membrane pores. However, they provide little information regarding the actual and dynamic absorption and build-up of fouling layers on the membranes due to the complicated convex surface of hollow fiber membrane. Compared to the other membrane configuration,

the hollow fiber membranes with a larger length-diameter ratio will result in the uneven axial fouling profile derived from the difference of the local TMP along the fiber. The challenge is to in-situ monitor membrane fouling deposition and distribution along a hollow fiber membrane during practical applications. Over the last decade, a number of non-invasive techniques have been developed for in-situ monitoring of the hollow fiber membrane fouling so that the formation and transport properties of foulants deposited on the membrane surface could be better understood as summarized in Table 1. The different principles and device specifics of these non-invasive techniques lead to different resolutions and technical features (Table 1). The application and contribution of these non-invasive techniques will be described in detail in the following subsections.

2.1. Direct observation technique

The direct observation (DO) technique is the most promising for direct and in situ observation of the foulants' deposition and its removal by optical probes [22]. This system consists of a microscope, a camera and a transparent membrane module. Generally, the microscope used in the DO apparatus is the upright optical bright-field microscope, which is the most elementary form of microscope illumination techniques and generally used with compound microscopes. Compared with the inverted microscope, the upright microscope is more suitable to observe the fouling deposition on the top surface of membrane. The objective lens of the microscope is focused on the permeate side of a transparent membrane. The wet membrane is transparent and thus the particle deposition can be observed. The DO

technique was firstly applied to visualize the deposition of yeast, latex particles or submicron bacteria on a flat sheet membrane [23-24].

The DO technique has been particularly successfully used when observing the yeast particles on the hollow fiber membrane surface [25]. The camera was concentrated on the edge of the hollow fiber membrane. It was found that the fouling of the transverse oriented fibers in the downstream context was dramatically reduced by compared to the upstream fibers in the cross-flow module. It was ascribed to the vortices between fibers, which swept the particles away from the face of the downstream fibers. Marselina et al. [26-27] further qualified the cake height using the DO technique and investigated the effects of cross-flow velocities and backwashing on the cake height, compressibility and specific resistance. In the viewing port, the hollow fiber membrane was dark and the model solution concerning the bentonite was light. Consequently, cake thickness was easily measured with the distinguishable boundary between the membrane and cake layer. The DO technique could distinguish the stagnant and fluidized cake layers deposited on the membrane surface. It firstly confirmed that the fouling layer consisted of both stagnant and fluidized cake layers. The fouling removal followed both the cake expansion and gradual erosion at low cross-flow velocity, but was subjected to the only direct erosion at a high cross-flow rate. In addition to estimating cake height, by using the DO technique, the effects of the hydraulic conditions [28], chemical environment [29], particle surface charge [30] and membrane structures [31] on the foulant layer growth, structure and compression/relaxation have been investigated. Although the DO technique does offer a good resolution (0.5 μm), it requires an appropriate transparent membrane or the feed solution to be clear enough.

2.2. Magnetic resonance imaging

Magnetic resonance imaging (MRI) as an on-line and non-invasive method can monitor the composition of a sample by measuring the distribution of mobile nuclei in any slice of the specimen [32-33]. For a decade, it has been extended to other areas like the flow visualization, concentration polarization and cake-layer formation in membrane processes [11, 34]. It should be noted that it was the first time to on-line visualize the fouling behavior inside the hollow fiber membrane using MRI technique [11]. When the entire shell of the test rig is exposed to a static magnetic field, the nuclei (i.e. the ^{1}H hydrogen nuclei) aligned with the field (Fig. 1a). Afterwards, a radio frequency pulse is applied, and this creates an oscillating magnetic field from the nuclei magnetization perpendicular to the main field. The nuclei reach an excited state by absorbing energy from the oscillating field. Then a signal is detected by the receiver coil when the nuclei return from the excitation state back to the equilibrium state. The characteristics of the signal (the amplitude of the induced radio frequency, voltage decay and the resonances against time) are a function of the individual properties of the specimen (e.g. the chemical environment and local diffusion coefficient). The signal can be transformed into images weighted by the longitudinal or transverse relaxation time. The intensity of this signal is proportional to the number of nuclei.

Buetehorn et al. [35] successfully applied the MRI technique to in-situ investigate the local cake growth during the submerged microfiltration of silica suspensions (Fig. 1b). When the difference between the particle concentrations in the cake layer and the bulk is significant, this will affect the relaxation properties of the protons. Thus, the cake layer appears as an

annulus of high signal intensity on the MRI images. Cake formation and removal can be visualized from the image analysis. It showed that the foulants preferentially deposited on the surface of hollow fiber membrane close to the suction end [35]. The rate of cake growth also rose when the permeate flux and the solids concentration increased. In addition, the cake-removal efficiency was enhanced with the increase of aeration pressure and duration of aeration. Çulfaz et al. [36] further investigated the fouling behavior of micro-structured hollow fibers and compared them to hollow fibers. Although more particles were deposited within the grooves of the micro-structured fibers, the cake layer formed was loose, which was more easily removed than the compact cake layer on the round fibers. MRI technique was successfully applied to measure the influence of Ca^{2+} on the fouling layer structure for the dead-end filtration of sodium alginate within the ceramic hollow fiber membranes [37]. MRI measurements reveal that the alginate layer in absence of Ca^{2+} resembles more a cake layer. However, the addition of Ca^{2+} led to a formation of a dense gel layer on the membrane surface.

Although the MRI as an online and non-destructive technique provides high quality images and makes flow analysis possible, it has a relatively low spatial resolution (10 μm), the device is specific and there is difficulty in extracting the best information.

2.3. X-ray microimaging

The phase-contrast X-ray imaging (XMI) with synchrotron radiation could be used to in-situ observe the membrane filtration processes. By compared to the MRI technique, XMI provides a high spatial resolution of 1 μm and approximately 1 s temporal resolution per

frame (Table 1). The XMI can be performed using the phase contrast imaging (PCI) beamline [38]. Fig. 2a illustrates the major components of the PCI beamline which include the Helios 2 synchrotron light source, beryllium filter window, sample holder, $CdWO_4$ scintillator, silicon mirror and charge-coupled device (CCD) camera. X-rays require a distinct difference in the electron density between the components of interest. When the X-rays pass through the sample, their amplitude and phase are influenced by the imaginary and real part of the refractive index, which is related to the material characterizations (e.g. density and light velocity in a medium, etc.). Based on this principle, Yeo et al. [39] employed the XMI technique to observe the cake layer in the fiber lumen and the particles deposited within the membrane pores during filtration of 1% iron hydroxide solution (Fig. 2b). A single hollow fiber membrane was held vertically in front of the scintillation foil. The hollow fiber before and after filtration was tested using XMI. The interface between the lumen and inner wall became more distinct and broader when the particles deposited on the fiber's inner face. The iron hydroxide particles can also be visualized within the pores. In sum, The XMI is a powerful tool for characterizing the membrane morphology. However, the XMI technique does require relatively expensive equipment and it is difficult to assess the cake's thickness.

2.4. Ultrasonic time-domain reflectometry (UTDR)

Ultrasonic time-domain reflectometry (UTDR) was first used by Greenberg et al. [40] to in-situ characterize the calcium sulfate scaling on the flat-sheet reverse osmosis (RO) membranes. Further, the UTDR technique as an in-situ, non-invasive and real-time technique has been applied to measure the compaction, fouling and cleaning of flat-sheet MF/UF/NF

(nanofiltration) membranes by our former and current group [41-43]. The general principle of the ultrasonic measurement is based upon the propagation of the mechanical waves [44]. When an ultrasonic wave encounters an interface between two media, the energy will be partitioned so that a reflected wave occurs. The amplitude of the reflected wave, relative to the incident wave, depends on the acoustic impedance (W) difference between the media. W is defined as $W=V\rho$, where V and ρ are the velocity and density of sound wave in the medium, respectively. A more significant ΔW between two media will lead to larger amplitude of the reflected signal from their interface.

The great challenge is to employ UTDR to monitor membrane fouling in tubular or hollow fiber membrane processes owning to their tubular or curve structure with many complicated interfaces. Interestingly, Xu et al. [45] reported the non-invasive monitoring of particle deposition on membrane surface in a module with a single hollow fiber membrane. The schematic diagram of UTDR measurement principle in a hollow fiber membrane module was shown in Fig. 3. To provide better a spatial resolution, a high frequency transducer of 10 MHz was externally mounted at the outside of the membrane module (Fig. 3a). The reflected signals D–G were generated from the following interfaces: water/upper outside surface of the hollow fiber, lumen upside surface/water, water/lumen underside surface and lower outside surface/water in the single hollow fiber membrane module. As the foulants deposited on the membrane surface, the acoustic impedance at the interface of the feed solution/membrane altered leads to the increase in the amplitude from peaks E to E' and F to F' (Fig. 3b). Once the fouling layer on the membrane surface was dense and thick enough, two reflected signals P and Q will be detected by the ultrasonic measurement system, and be generated from the

fiber lumen upside surface-fouling layer interface and the fiber lumen underside surface-fouling layer interface, respectively. If the difference of arrival times between signals P and E' is measured, the thickness of the fouling layer (*dS*) can be calculated by the following equation:

$$dS = 0.5 v_s dt \quad (1)$$

where v_s is the ultrasonic velocity in the fouling layer (m/s), *dt* is the difference in arrival time between the fouling layer and membrane echo signals (s). This study confirmed that UTDR measurement could provide a new protocol for the observation of hollow fiber membrane fouling and cleaning.

In order to further improve the sensitivity and realize the visualization of membrane fouling monitoring, Xu et al. [46] incorporated Fourier wavelet transform into UTDR technique to visualize the fouling deposition and distribution along the outside surface of the hollow fiber membrane using three 10 MHz ultrasonic transducers as shown in Fig. 4. The advantage of the Fourier wavelet transform method is that it can visually present individual peaks from the different surfaces through 2D and 3D images. In addition, the differential signal technique was applied to analyze the fouling reflection signals, which was equal to the difference between the reference and test waveforms, representing the echo signal of the fouling layer. When using differential signals and wavelet technique, the resolution of UTDR measurements could research to h/λ=0.04, where *h* is the layer thickness and λ is the wavelength [44]. It could provide more information from fouling signals. Fig. 4 shows that the acoustic duration time of the fiber lumen upside and underside surfaces increased from

0.69 to 0.84 μs and from 0.75 to 1.08 μs as the fouling progressed, respectively. The wavelet analysis of the ultrasonic spectra demonstrated that the diameter of the fiber lumen decreased due to the deposition of foulants. Especially, the oil diffusion behavior including relaxation and disappearance was firstly visualized by UTDR technique in real time after the microfiltration system was shut down.

Specifically, UTDR coupled with differential signal technique demonstrates a vital role in monitoring fouling behavior under sub-critical flux operation with different module configurations. For instance, Li et al. [47] for the first time on-line monitored the fouling distribution along the submerged hollow fiber membrane under the sub-critical flux operation by UTDR coupled with differential signal technique. It was found that fouling still occurred even under sub-critical flux operation with a dead-end submerged hollow fiber membrane (SHFM) module. The progress of foulant deposition onto the membrane surface gradually migrated from the top to bottom in the vertical one-end module. Increasing the aeration rate from 15 to 45 ml/min could only reduce fouling but could not completely eliminate it. Similarly, decreasing the fiber length (from 1.0 to 0.6 m) had a negligible effect on the membrane fouling control [47]. Further, Li et al. [48-49] investigated the effect of the module configuration (horizontal double-end and vertical double-end modules) on fouling behavior using UTDR technique. The acoustic measurements revealed that the suction ends of the double-end SHFM module were fouled more easily than the middle part of the module. The horizontal configuration showed a more uniform fouling distribution than the vertical configuration. For the vertical configuration, the upper suction end was fouled more severe

than the lower suction end.

Obviously, as a powerful in-situ and non-invasive technique, the distinct advantage of UTDR technique is that it is one of the few in-situ techniques potentially applicable to commercial-scale membrane modules and processes, serving as a new approach for module optimization to reduce membrane fouling. However, the propagation of acoustic waves in the multilayer membrane structure requires further investigations, so as to obtain more accurate and useful information from the complex ultrasonic spectra.

2.5. Electrical impedance spectroscopy

Electrical impedance spectroscopy (EIS) is a technique that has proved to be a powerful tool for in-situ and invasive monitoring membrane fouling processes [50]. Evidently, the EIS technique is sensitive to variations in the structures of membranes and makes it possible to determine individual conductance and capacitances of the membrane surface. The electrical impedance (EI) is defined as the ratio of a voltage to its corresponding current as well as the phase difference between them [51]. Generally, the EIS units mainly consist of electrodes in the feed and permeate solutions, and an external electrical contact with the edges of the membrane injecting currents into the membrane. The corresponding current and voltage as well as the phase difference throughout the membrane are measured using digital techniques. When the foulants accumulate on the membrane surface, the conductive and capacitive properties of the interface region will change. Hence, any variation in the dispersion of the capacitance and conductance with frequency provides a method of in-situ monitoring of the accumulation of foulants on the membrane surface.

Recently, Bannwarth et al. [52] firstly extended the EIS technique from the flat-sheet membrane to the hollow fiber membrane using a 2-terminal method. To perform EIS on a hollow fiber membrane, a special module was designed and constructed. The principles of the measurement are described in Fig. 5a. A wire-shaped electrode was positioned inside the hollow fiber membrane and a ring-shaped electrode was located around the outside of the membrane. The impedances could be measured using an alternating current (AC) field applied in the radial direction between two electrodes since the system was immersed in an electrolyte solution (Fig. 5b). The magnitude of the impedance rose with the increase in the membrane porosity. A model was further developed to confirm the high consistency between the experimental data and theoretical assumption.

Bannwarth et al. [53] further successfully used EIS to on-line monitor the cake layer structure on the hollow fiber membrane during fouling experiments with silica particles in the inside-out dead-end filtration mode. The impedance measurement could be used to determine the cake layer thickness as well as porosity. It revealed that the cake layer porosity increased with proceeding filtration. The above studies have confirmed that the impedance spectroscopy is a powerful tool to characterize the hollow fiber membrane. It is worth noting that the EIS method requires a specific module to bond the metal film on the membrane surface and alter the membrane structure.

2.6. Streaming potential measurement

Generally, the membrane fouling depends on not only the hydrophilicity/hydrophobicity but also the electrokinetic properties of the membrane. The streaming potential measurement

is widely used to characterize the electrokinetic properties of membranes, including both the electric properties of the pore wall and outer surface, described by the transversal and tangential streaming potentials, respectively. Fouling would alter the electric properties of the membrane, leading to changes in the streaming potential. Thus, it allows membrane fouling to be monitored with a high sensitivity. The zeta potential can be calculated using the Helmholtz–Smoluchowski (H–S) relationship which is derived from the tangential streaming potential or streaming current measurements.

Chun et al. [54] studied the variation of the zeta potential during membrane filtration of colloidal suspensions. The zeta potential variation was directly linked to the colloid deposition on the membrane surface, which varied more significantly at the inlet than at the outlet, suggesting an axial-position-dependent fouling layer along the hollow fiber membrane. Similarly, Sung et al. [55] investigated the variation of the streaming potential coefficient during filtration of the bovine serum albumin (BSA) solution. The streaming potential became more negative as the filtration progressed in the case of pH 10. This indicated that the electrostatic repulsion between the BSA molecules existed mainly within the concentration polarization layer rather than the deposition at the outer membrane surface.

In order to avoid the installation of internal electrodes into the hollow fiber membrane, Fievet et al. [56] firstly executed the tangential electrokinetic measurements on the hollow fiber membrane using a custom-made module. A rod-type Ag/AgCl electrode was positioned 2 cm away from the end of the fibers. Another disk-shaped Ag/AgCl electrode was located about 5 mm away from the end of the tube (Fig. 6). Both the tangential streaming potential and streaming current changed linearly with the pressure difference even when there was no

fully laminar flow [56]. Furthermore, Jia et al. [57] demonstrated that the zeta-potential varied depending on the fouling mechanisms (Fig. 7). The zeta potential declined rapidly in the pore blocking process, but decreased gradually and linearly during the cake formation process, whereas it was almost stable in the cake compression process. Different from most studies using single model foulant (e.g. latex particles, BSA, et al.), Wang et al. [58] performed zeta potential measurement using real raw water to monitor membrane fouling. They found that the apparent zeta potential was a useful indicator for fouling in both the direct submerged hollow fiber membrane filtration and in-line coagulation ultrafiltration. In addition, this indicator could also be used to monitor fouling removal during backwashing.

Overall, the streaming potential measurement is a simple and powerful tool for in-situ monitoring the hollow fiber membrane. This is despite the fact the technique needs to use the specified measuring cell and depends on the significant difference between the charges of the foulants and membrane.

3. In-situ monitoring techniques for local filtration characteristics

The local filtration hydrodynamics can significantly affect membrane fouling and system operation stability. Direct and rigorous monitoring of local filtration hydrodynamics during membrane filtration can provide useful information to better understand the filtration phenomenon and guide fouling control. Generally, to understand the local filtration hydrodynamics at different positions along a hollow fiber membrane, the hollow fiber is cut into the different segments at regular intervals after the filtration process to measure the permeate flux of each segment. However, this method would modify the structures of the

membrane and the fouling layer as a result of depressurization and movement. To accurately characterize the local filtration behavior at a given time during filtration, the only way is to use an in-situ and non-invasive measurement method, which will not interfere with the build-up and removal of the fouling layer. Therefore, a number of monitoring techniques have been proposed to provide direct and dynamic insights into the flow characterization of the hollow fiber membranes during the last decades as listed in Table 2.

3.1. Experimental segmentation method

Some experimental methods have been conducted by dividing the filtrate compartment into subcompartments separated using watertight partitions. These techniques can only give a quasi-local measurement of the filtration flux because each subcompartment has a specific length [59]. For example, Yoon et al. [60] cut the hollow fiber membrane into eight 250-mm pieces with a 20 mm T-connector connecting every two adjacent pieces (Fig. 8a). 5 mm of each piece was inserted into the T-connector glued by the epoxy resin, forming a 10 mm internal space for the permeate to flow. A transparent flexible PVC tube was connected with the T-connector for pressure reading in the node. The experimental pressure profiles were found to well agree with the theoretical values calculated using Hagen–Poiseuille equation when deionized water was filtered (Fig. 8b). This method was further used to monitor the internal pressure profile along the fiber during the filtration of activated sludge, demonstrating that the local flux near the membrane outlet was not the highest owning to the collapse of the cake layer.

Lee et al. [61] developed another experimental method to determine the local flux profile along a horizontal hollow fiber membrane. The local TMP was then calculated using the resistance-in-series model. This system consisted of three parallel hollow fiber membranes. Each single hollow fiber was placed into five compartments (C1-C5) (Fig. 9). The left end of each fiber was sealed while the other end was connected by a silicon tube which extended to the suction pump. The variations in the water level after filtration operation were used to calculate the local permeate flux and its distribution. This method was also related to the measurement of the local bio-layer porosity profile using a Confocal Laser Scanning Microscope (CLSM). It indicated that there was a good correlation between the local bio-cake porosity and local TMP. Wang et al. [62] investigated the effects of the backflushing flow rate and pressure on the local permeate flux using a similar method. The permeate flow was found to decrease from the outlet to the dead-end as backflushing processed. With an increase in membrane length, a higher backflushing flowrate (pressure) was required to achieve the same cleaning outcome. Meanwhile, the optimized backwashing time firstly increased and then decreased as the backwashing flow rate (pressure) increased.

Similarly, Li et al. [63] proposed an experimental method to measure the local flux profile in a submerged hollow fiber membrane module. The feasibility of this technique was validated by the small root mean square error (17.4 %) between the experimental and simulated local fluxes. Generally, the permeate can be sucked from either one end or both

ends of hollow fibers. Thus, the configuration of the submerged hollow fiber membrane (SHFM) module can be divided into the dead-end and double-end membrane modules. Results showed that the local flux distribution in the double-end submerged hollow fiber membrane module was more uniform than that in the dead-end module (Fig. 10). Thus, the double-end submerged hollow fiber membrane module such as GE's ZeeWeed series module is a typical configuration used in the industrial systems. In the double-end module, the local flux obtained at the upper suction end was higher than that at the lower suction end, and the difference between them decreased at a lower average operating flux and a shorter fiber length. The local flux distribution measured by this method correlated well with the fouling distribution obtained by the ultrasonic technique.

These experimental methods based on segmentation are practical and inexpensive. The usual relative error is within a margin of 20 %. Thus, it has been used to validate the modeling of local flux distribution in hollow fiber membrane module. To further accurately determine the local filtration flux, some online and non-invasive monitoring methods are proposed using below the specified equipments.

3.2. Magnetic resonance imaging

The principle of MRI is based on the amplitude of the radio frequency, voltage decay and resonances against time under different hydrodynamic environments, which has been described in detail in section 2.2. In the early studies by Pangrle et al. [64-65], the MRI technique was employed to obtain fluid flow patterns in the hollow fiber modules. The inlet flow patterns changed significantly with the variation in Reynolds number. The

maldistribution of flow existed in the whole module. Similarly, Heath et al. [33] applied the MRI to monitor the starling flows in the shell side of hollow fiber membrane modules in bioreactors. The experimental axial velocity profiles fit with the theoretical predictions obtained from Poisson's equation. Except for measuring the flow velocity and distribution, it also could be used to visualize the development of oil polarization layers in the outer surfaces of the hollow fibers during filtration of an oil/water emulsion [66]. It further confirmed that the permeate flux is mainly controlled by the hydraulic resistance of the oil layer.

Specifically, MRI was employed by Laukemper-Ostendorf et al. [67] to visualize the flow velocity profile in hollow fiber hemodialyzers. The MRI measured not only the flow velocities in the fiber lumen but also the dialysate flow through the fibers. Further, using MRI, Hardy et al. [68] found that the local flux decay accompanied by the linear decrease in the local pressure drop along the fiber. In particular, Osuga et al. [69] successfully detected a small degree of non-uniformity in the dialysate flow in a hollow fiber dialyzer using Gadolinium (Gd) as paramagnetic ions, which was ascribe to the local non-uniformity of the hollow fiber density and vortex generation in the dialysate flow. The application of MRI also revealed that the installation of an appropriate baffle could enhance mass transfer at the dialysate side and improve the uniformity of the dialysate flow [70].

Recently, Buetehorn et al. [35] utilized the MRI to non-invasively visualize both the distribution of local permeate flux and local cake growth along the submerged hollow fiber membrane module during filtering silica suspensions. The results showed that the local permeate flux increased linearly from the dead-end to the suction end of the module. The formation of heterogeneous cakes was observed with a greater thickness close to the suction

end. Further, the fouling growth rate was directly related to the permeate flux and solids concentration. Apart from this, the flow imaging in the membrane distillation hollow fiber modules has been carried out to explore the effects of different configurations (randomly-packed, spacer-knitted, curly and semi-curly fibers) on internal flow hydrodynamics [71]. The curly-fiber module exhibited better transverse flow compared to the randomly-packed module. In the spacer-knitted module, the stagnant zones were reduced significantly as a consequence of the flow channel in the center of the module resulting in significant transverse flow. The MRI is a unique technique to both monitor the flow behavior and fouling deposition, especially in the irregular structured hollow fiber membrane. It is worth noting that the permanent magnet of a low-field MRI instrument is only 0.3 T in this study. Although this system has poorer imaging quality compared with the typical high-field MRI system (>4.7 T), it is not expensive and more mobile.

3.3. Constant temperature anemometer

The on-line and non-invasive constant temperature anemometer (CTA) technique has been successfully used in the velocity and wall shear force measurements as well as in two-phase or multiphase flows because of high sensitivity and relative low cost [72]. Recently, CTA has also been used to study fluid velocities in membrane-based separation [73-75]. The primary principle of its operation is based on the convective heat transfer from the heated element to the surrounding fluid. Any changes in the fluid velocity will alter the convective heat transfer coefficient and thereby affect the sensor temperature. To maintain the temperature, the electric current supplied to the sensor will change to achieve a new equilibrium. Thus the

variation in the current applied to the sensor can be associated with the changes in fluid velocity.

Le-Clech et al. [76] firstly incorporated CTA technology into membrane channels to precisely measure the local flow velocity. The potential of the CTA sensor was confirmed for the measurement of the velocity distribution in a spacer-filled channel fed with pure water or solutions containing dissolved solutes, and in the submerged membrane module with air sparging. Wicaksana et al. [77] further applied the CTA technique to determine the flow distribution among hollow fiber bundles in a submerged membrane module (Fig. 11a). Five CTA sensors were located in a matrix above the outlets of the fibers so that the individual permeate flow of each fiber could be monitored. Results revealed that the mal-distribution of flow among the fiber bundles, which was related to the non-uniform cake deposited on the membrane surface and uneven aeration (Fig. 11b). The CTA technique provided a very sensitive tool for filtration performance monitoring. However, it is also fragile and easily affected by environmental changes in addition to fluid velocities.

3.4. Doppler ultrasonography

Pulse Doppler ultrasonography was successfully used to precisely evaluate the internal filtration flow rates of the dialyzer based on the Doppler Effect [78-79]. The Doppler Effect is a well-known phenomenon in which the motion of the source of a sound in relation to a receiver causes an apparent change in the frequency of the sound that can be measured. As shown in Fig. 12, the Doppler shift is defined as the difference between the transmitted and

observed frequencies of the ultrasound beam. Thus, the average velocity of blood flow in a cross-sectional plane in the dialyzer could be calculated by the Doppler shift equation:

$$f_D = \frac{2Vf_r \cos\theta}{c} \quad (2)$$

where f_D is the Doppler shift (Hz), f_r is the frequency transmitted by the transducer (Hz), V is the blood flow velocity (m/s), c is the velocity of the sound beam (m/s), and θ is the angle of the insonation.

Herein, Mineshima used the pulse Doppler ultrasonography to estimate the internal filtration flow rate and the blood flow velocity in the hollow fibers of dialyzers [80]. A good correlation emerged between the observed blood velocity and blood flow rate at the inlet portion of the dialyzers using bovine blood. The blood flow rate profiles along the dialyzer could be estimated from the blood velocity and the total cross-sectional area of the hollow fiber membranes. Further, Mineshima and Sakiyama et al. extensively used the Doppler ultrasonography to investigate the effect of blood flow rate on the internal filtration in a high-flux dialyzer [81]. Results showed that the internal filtration flow rate increased with the increase of the blood flow rate. Although Doppler ultrasonography can be very useful for monitoring the local internal filtration flow, to date it has only been used for the dialyzer.

3.5. Scintigraphic technique

As an on-line and non-invasive visualization technique, the scintigraphic technique could directly measure the local solute concentration and determine the local filtration flux without destroying or transforming the filter [82-83]. During the monitoring process,

macroaggregates (eg. ^{99m}Tc albumin, etc.) are able to be utilized as marked molecules to be mixed with main blood. It should be noted that the marked molecules can not disturb the flow inside the hollow fibers. Since the marked molecules are too big to cross the dialysis membrane, its concentration change is assumed to be related to the changes in the blood content. As a consequence, the protein concentration in the bulk fluid is proportional to the marker concentration and to its radioactivity $\gamma(x)$. The relationship is obtained as follows:

$$c_b(x) = \frac{\gamma(x)}{\gamma(0)} c_{bi} \tag{3}$$

where γ is the radioactivity of the radiolabeled marker (Bq), c_b is the local bulk protein concentration (kg/m^3), and c_{bi} is the local bulk protein concentration at the hemofilter's inlet/outlet (kg/m^3).

These changes in concentrations recorded by a gamma camera could be evaluated to establish the cumulative values of filtration and its profiles along the fiber. In addition, the local filtration flux can be calculated using the differentiating concentration profiles and mass conversation. The mass conservation of the radiolabeled marker and the continuity of an incompressible fluid can be expressed as follows:

$$Q(x) c_b(x) = Q_i c_{bi} \tag{4}$$

$$2\pi N R_i J_i(x) = -\frac{dQ(x)}{dx} \tag{5}$$

where Q is the flow (m^3/s), Q_i is the inlet flow (m^3/s), N is the number of fibers, R_i is the fiber inner radius (m) and $J_i(x)$ is the local flux at x coordinate.

The local filtration flux (J_i) was obtained after differentiating (Eq. (4)) with respect to x

$$J_i(x) = -\frac{Q_i}{2\pi N R_i}\frac{d}{dx}\left[\frac{c_{bi}}{c_b(x)}\right]$$

$$= -\frac{Q_i}{2\pi N R_i}\frac{d}{dx}\left[\frac{a(0)}{a(x)}\right] \quad (6)$$

Ronco et al. [84] used the scintigraphic technique to measure the variation of the protein concentration and local filtration flux along the fiber during the UF of blood solutions. The local flux was calculated using a linearized relationship, whereas this calculation method was only valid for the low filtration flux. To further investigate the filtration behavior of the high-permeability membrane, Defossez et al. [85] examined the spatial variation of protein concentration and local filtration flux calculated by an exact nonlinear relation using the scintigraphic technique. The monitoring data confirmed that the local filtration flux decreased from the inlet to the outlet. There existed a high retrofiltration rate in the downstream part of the fibers in the case of large filtration flux, which was ascribed to the high osmotic pressure at the membrane surface resulting from the protein polarization concentration. In addition, the scintigraphic technique as a promising and non-destructive tool has been used for optimization and assessment of hollow fiber dialyzers [86-88]. However, the scintigraphic technique is similar to Doppler ultrasonography, which has only been used for the dialyzer.

3.6. Particle image velocimetry

Particle image velocimetry (PIV) is a non-invasive technique for investigation of spatial flow structures in both steady and unsteady flows. It has been widely used in the study of fluid flows from artificial heart valves to rockets [89-90]. The general principle of PIV is to illuminate the tracer particles in a flow field using a laser sheet, and then acquire two images

of the diffracted light pattern of the particles with a known time interval. The density of tracer particle should be similar to the density of solution so that the particles are essentially neutrally buoyant. The displacement of the particles is obtained by cross-correlating the two images and with the known time interval. The velocity vector field can also be determined.

Based on this principle, Yeo et al. successfully used the laser imaging technique of PIV to measure the local velocities around a hollow fiber array [91-92]. The effects of the characteristics of air sparing on filtration performance were investigated in their studies. They found that many small bubbles can be more effective for fouling control than a few large bubbles at the same aeration flow rate. The rate of TMP rise during constant flux experiments can be correlated to both the mean shear and turbulence kinetic energy around the fibers induced by the bubbling. To further investigate the effect of hydrodynamics induced by aeration on the membrane fouling behavior, the filtration experiments coupled with PIV technique and CFD numerical simulation were employed to investigate both wall shear stress and liquid flows along the membrane surface [93]. Experimental results demonstrated that filtration performances were mainly controlled by local air flow rate rather than the kind of bubbles. Additionally, the effect of turbulence on submerged hollow fiber membrane filtration was comprehensively examined by Pourbozorg et al [94]. The non-invasive laser imaging approach of PIV was used to quantify the characteristics of the ambient turbulence. Their study demonstrated that the fouling rate generally decreased with an increase in turbulence kinetic energy and integral length scale. However, if it is beyond an optimal value of the integral length scale, the fouling rate did not reduce any further. Consequently, there exists an optimal turbulence length scale (approximately ten times of the hollow fiber diameter) for

membrane fouling control.

To confirm that mechanical vibration of vertical hollow fibers can improve the membrane filtration, the turbulence induced by the holding frame vibration was examined using the technique of PIV [95]. PIV measurements revealed that the turbulence generated by the holding frame was more obvious at higher vibration frequencies. Recently, PIV technique was used to validate CFD modeling of hydraulic properties of membrane bioreactors through determination of liquid velocity in bubbly flow [96-97]. This ensured that the CFD simulations could accurately predict the effects of aeration system, membrane module configuration and filtration tank geometry on the hydrodynamics and aeration patterns in a pilot scale membrane bioreactor. Although PIV technique is only applied in the transparent filtration system, it is still a powerful experimental tool to study the hydrodynamics within a hollow fiber bundle.

4. Future R&D direction

Although tremendous efforts have been made to develop on-line monitoring techniques and methods, many of them are still limited to the laboratory for the investigations of fouling development and dynamics in hollow fiber membrane processes. Until recently, PIV imaging technique has been used to investigate the hydrodynamics in the pilot-scale submerged hollow fiber membrane module. Consequently, more attention should be paid to the main gap between the current state-of-the-art and the large–scale application so as to develop some strategies to tackle the challenges.

4.1. Future challenges for fouling monitoring techniques

Most of the technologies of fouling monitoring are hard to be employed as a monitoring tool for fouling in the commercial membrane module with thousands hollow fibers. The limitations are ascribed to three aspects: specify membrane module, high specificity of device and data processing technology. For instance, direct observation technique is limited by not only the specify module (transparent module and clear feed solution), but also the image resolution. Especially, when the light diffusion and subsequent absorption occur at the interfaces of multiple fibers, it is hard to detect the fouling deposition inside the fiber bundle. Maybe fluorescence labeling can be used to enhance optical intensity or the use of confocal laser microscopy may increase the precision and depth resolution. Similarly, acoustic reflection, refraction and absorption from fine hollow fibers limit the penetration of UTDR in the commercial module. This can be mitigated somewhat by using a focused transducer. Importantly, it is hard to extract useful fouling information due to signal interpretation resulted from multiple reflections from many interfaces in a hollow fiber membrane module. Thus, the development of a comprehensive acoustic model coupled with advanced signal processing technology such as Fourier transforming is useful for the potentials in the application of commercial module.

Unlike the above low complex instruments, the MRI and XMI techniques are extremely restrictive to the highly specific equipments. Especially, the size of these devices available significantly restricts the application in the field of the commercial membrane module. However, the electrical impedance spectroscopy generally requires a specially designed membrane cell to position an electrode inside the hollow fiber membrane and bond an

electrode around outside of membrane. Thus, it is difficult to be applied in the practical application.

Moreover, streaming potential measurement as a simple tool is one of the few noninvasive methods potentially applicable to the commercial-scale modules. Recently, Wang et al. performed zeta potential measurement to monitor the membrane fouling in-situ in the process of coagulation/flocculation ultrafiltration with an experimental-scale module [58]. It confirmed that the apparent zeta potential could be a useful indicator for monitoring membrane fouling. To improve monitoring sensitivity, a stable and sensitive electrode is necessary for the commercial application. However, it can only provide integrative fouling information, rather than the local fouling property. Thus, the integration of multiple techniques is a promising strategy for the fouling monitoring in the commercial application.

Although it is difficult in practice for monitoring local fouling properties in a commercial module, an alternation approach is to use a side-stream cell along the commercial hollow fiber membrane module elements under the same operating conditions. With the integration of monitoring technique, such as non-invasive UTDR, DO technique or EIS etc., the side-stream cell is capable to provide an effective early warning of membrane fouling. This strategy has been successfully used to monitor fouling and cleaning of the reverse osmosis spiral wound module [98-99]. It confirmed that the side-stream cell coupled with UTDR could monitor membrane fouling and cleaning in a commercial spiral wound module.

4.2. Future challenges of monitoring techniques for filtration characteristics

The experimental segmentation method is simple and suitable to the investigation of

filtration behavior of membrane module with a single hollow fiber. It could not be used in commercial module. The MRI imagining is still not suitable to the hydrodynamics investigation of the large-scale hollow fiber membrane module because of the size limit of highly specific equipment as described in Section 4.1. However, the scintigraphic technique and Doppler ultrasonography have been used for the dialyzer.

In addition, among these techniques, the CAT and PIV techniques have a potential to monitor the flow rate inside hollow fiber membrane and local velocity changes around fiber bundle in the large-scale membrane system, respectively. Especially, PIV imagining technique has been successfully used in a commercial-scale submerged hollow fiber membrane module [96-97]. PIV imagining technique combined with CFD modeling illustrated the effects of membrane module configuration and aeration patterns on the local velocities and shear forces in the membrane bioreactors. However, CAT technique still faces some challenges including be fragile and sensitive to environmental changes of CAT sensors. This is because the CAT sensors have to face the complex running environmental and frequent encounters with particles or contaminants in practical application. It would affect the accuracy and damage the sensor. To reduce this risk, reducing sensor footprint or increasing settlements of more sensors within module is a promising strategy.

5. Concluding remarks

The in-situ monitoring techniques for membrane fouling and local filtration behaviors in the hollow fiber membrane process have critically reviewed. Although these in-situ fouling monitoring techniques provide new insights into the membrane fouling and control

mechanisms, they are mainly used in the lab-scale experiments. It is of great significance to broaden their application areas into the industrial processes with long-term filtration, where membrane fouling is often more severe due to the unstable feed properties and the seasonably varied environmental conditions, so that it could be extensively used in the design of membrane modules. Also, new on-line monitoring devices with faster data analysis and ease of operation need to be developed to satisfy the complex and various demands in the industrial application. Meanwhile, several existing techniques still need refinements to improve the accuracy and resolution by improving the optics, spectroscopy and sensors to provide more information within the concentration polarization layer with only a few micrometers at the membrane surface.

The observations of local filtration and hydrodynamic behaviors in the hollow fiber membrane module can help us to deeply understand changes occurring in the local hydrodynamic properties along the fiber axial direction. From these fouling control strategies could be developed. However, any single existing technique cannot monitor the overall hydrodynamic characteristics during filtration processes. Novel techniques are needed with the potential to readily provide comprehensive hydrodynamic information from commercial modules during the practical applications. The combination of a variety of techniques can integrate their individual advantages to eliminate weaknesses, thus providing more accurate and comprehensive information. In addition, the combination of theoretical prediction and experimental observation could provide deeper understanding of the fluid hydrodynamic conditions. Thus, these in-situ monitoring technique combined with filtration hydrodynamics models is a promising and attractive method for the design and optimization of the membrane

module during practical applications.

In summary, a comprehensive understanding of the relationship between local fouling and hydrodynamics is a critical issue for fouling control strategies and proper module design, so that existing obstacles can be successfully overcome.

Acknowledgments

This work was financially supported by the Chang-jiang Scholars and Innovative Research Team at the University of Ministry of Education of China (Grant No. IRT13084) and the Science and Technology Research Programs of Tianjin, China (Grant no. 15PTSYJC00240). It was also supported in part at the Technion by a Technion-Guangdong Fellowship and the Helmsley Charitable Trust.

References

[1] J.Y. Tian, H. Liang, J. Nan, Y.L. Yang, S.J. You, G.B. Li, Submerged membrane bioreactor (sMBR) for the treatment of contaminated raw water. Chem. Eng. J. 148 (2009) 296–305.

[2] L. Ma, B.H. Su, C. Cheng, Z.H. Yin, H. Qin, J.M. Zhao, S.D. Sun, C.S. Zhao, Toward highly blood compatible hemodialysis membranes via blending with heparin-mimicking polyurethane: Study in vitro and in vivo, J. Membr. Sci. 470 (2014) 90–101.

[3] K. Xiao, Y. Xu, S. Liang, T. Lei, J.Y. Sun, X.H. Wen, H.X. Zhang, C.S. Chen, X. Huang, Engineering application of membrane bioreactor for wastewater treatment in China:

Current state and future prospect, Front. Environ. Sci. Engin. 8 (2014) 805–819.

[4] S.H. Yoon, Membrane Bioreactor Processes—Principles and Applications, CRC Press, New York, USA, 2016, Chapter 6, pp. 253–331.

[5] Bue T., Cumin J., MBR module design and operation, Desalination 2010, 250: 1073–1077.

[6] Z.W. Wang, Z.C Wu, X. Yin, L.M. Tian, Membrane fouling in a submerged membrane bioreactor (MBR) under sub-critical flux operation: Membrane foulant and gel layer characterization, J. Membr. Sci. 325 (2008) 238–244.

[7] J.Y. Sun, K. Xiao, Y.H. Mo, P. Liang, Y.X. Shen, N.W. Zhu, X. Huang, Seasonal characteristics of supernatant organics and its effect on membrane fouling in a full-scale membrane bioreactor, J. Membr. Sci. 453 (2014) 168–174.

[8] V. Chen, H. Li, A.G. Fane, Non-invasive observation of synthetic membrane processes – a review of methods, J. Membr. Sci. 241 (2004) 23–44.

[9] J.C. Chen, Q.L. Li, M. Elimelech, In situ monitoring techniques for concentration polarization and fouling phenomena in membrane filtration, Adv. Colloid Interface Sci. 107 (2004) 83–108.

[10] E. Kujundzic, A.R. Greenberg, M. Peterson, Review: ultrasonic characterization of membranes, Desalin. Water Treat. 52 (2014) 1217–1249.

[11] C. Güell, M. Ferrando, F. López, Monitoring and Visualizing Membrane Based Processes, Wiley-VCH Verlag GmbH & Co. KGaA, Weinheim, 2009.

[12] J. Kim, F.A. DiGiano, Fouling models for low-pressure membrane systems, Sep. Purif. Technol. 68 (2009) 293–304.

[13] W.X. Zhang, J.Q. Luo, L.H. Ding, M.Y. Jaffrin, A Review on Flux Decline Control Strategies in Pressure-Driven Membrane Processes, Ind. Eng. Chem. Res. 54 (2015) 2843–2861.

[14] J. Zhang, H.C. Chua, J. Zhou, A.G. Fane, Factors affecting the membrane performance in submerged membrane bioreactors, J. Membr. Sci. 284 (2006) 54–66.

[15] S. Chang, A.G. Fane, The effect of fibre diameter on filtration and flux distribution—relevance to submerged hollow fibre modules, J. Membr. Sci. 184 (2001) 221–231.

[16] M. Lee, J. Kim, Analysis of local fouling in a pilot-scale submerged hollow-fiber membrane system for drinking water treatment by membrane autopsy. Sep. Purif. Technol. 95 (2012) 227–234.

[17] T. Carroll, The effect of cake and fiber properties on flux declines in hollow-fiber microfiltration membranes, J. Membr. Sci. 189 (2001) 167–178.

[18] A.H. Konsowa, M.G. Eloffy, Y.A. El-Taweel, Treatment of dyeing wastewater using submerged membrane bioreactor, Desalin. Water Treat. 51 (2013) 1079–1090.

[19] Q.H. Xu, Y. Ye, V. Chen, X.H. Wen, Evaluation of fouling formation and evolution on hollow fibre membrane: Effects of ageing and chemical exposure on biofoulant, Water Res. 68 (2015) 182–193.

[20] F. Xiao, P. Xiao, W.J. Zhang, D.S. Wang, Identification of key factors affecting the organic fouling on low-pressure ultrafiltration membranes, J. Membr. Sci. 447 (2013) 144–152.

[21] Y. Hao, C. Liang, A. Moriya, H. Matsuyama, T. Maruyama, Visualization of protein

fouling inside a hollow fiber ultrafiltration membrane by fluorescent microscopy, Ind. Eng. Chem. Res. 51 (2012) 14850–14858.

[22] P. Le-Clech, Y. Marselina, Y. Ye, R.M. Stuetz, V. Chen, Visualisation of polysaccharide fouling on microporous membrane using different characterisation techniques, J. Membr. Sci. 290 (2007) 36–45.

[23] H. Li, A.G. Fane, H.G.L. Coster, S. Vigneswaran, Direct observation of particle deposition on the membrane surface during crossflow microfiltration, J. Membr. Sci. 149 (1998) 89–97.

[24] H. Li, A.G. Fane, H.G.L. Coster, S. Vigneswaran, An assessment of depolarization models of crossflow microfiltration by direct observation through the membrane, J. Membr Sci. 172 (2000) 135–147.

[25] S. Chang, A.G. Fane, S. Vigneswaran, Experimental assessment of filtration of biomass with transverse and axial fibres, Chem. Eng. J. 87 (2002) 121–127.

[26] Y. Marselina, P. Le-Clech, R. Stuetz, V. Chen, Detailed characterisation of fouling deposition and removal on a hollow fibre membrane by direct observation technique, Desalination 231 (2008) 3–11.

[27] Y. Marselina, Lifia, P. Le-Clech, R.M. Stuetz, V. Chen, Characterisation of membrane fouling deposition and removal by direct observation technique, J. Membr. Sci. 341 (2009) 163–171.

[28] Y. Ye, V. Chen, P. Le-Clech, Evolution of fouling deposition and removal on hollow fibre membrane during filtration with periodical backwash, Desalination 283 (2011) 198–205.

[29] Q.H. Xu, Y. Ye, V. Chen, X.H. Wen, Evaluation of fouling formation and evolution on hollow fibre membrane: Effects of ageing and chemical exposure on biofoulant, Water Res. 68 (2015) 182–193.

[30] S. Lorenzen, Y. Ye, V. Chen, M.L. Christensen, Direct observation of fouling phenomena during cross-flow filtration: Influence of particle surface charge, J. Membr. Sci. 510 (2016) 546–558.

[31] P.Z. Çulfaz, M. Haddad, M. Wessling, R.G.H. Lammertink, Fouling behavior of microstructured hollow fibers in cross-flow filtrations: Critical flux determination and direct visual observation of particle deposition, J. Membr. Sci. 372 (2011) 210–218.

[32] B. Blümich, NMR Imaging of Materials, Clarendon Press, Oxford (UK), 2000.

[33] C.A. Heath, G. Belfort, B.E. Hammer, S.D. Mirer, J.M. Pimbley, Magnetic resonance imaging and modeling of flow in hollow-fiber bioreactors, AIChE J. 36 (4) (1990) 547–558.

[34] B.E. Hammer, C.A. Heath, S.D. Mirer, G. Belfort, Quantitative flow measurements in bioreactors by nuclear magnetic resonance imaging, Biotechnology 8 (1990) 327–330.

[35] S. Buetehorn, L. Utiu, M. Küppers, B. Blümich, T. Wintgens, M. Wessling, T. Melin, NMR imaging of local cumulative permeate flux and local cake growth in submerged microfiltration processes, J. Membr. Sci. 371 (2011) 52–64.

[36] P.Z. Çulfaz, S. Buetehorn, L. Utiu, M. Kueppers, B. Bluemich, T. Melin, M. Wessling, R.G.H. Lammertink, Fouling behavior of microstructured hollow fiber membranes in dead-end filtrations: critical flux determination and NMR imaging of particle deposition, Langmuir 27 (2011) 1643–1652.

[37] F. Arndt, U. Roth, H. Nirschl, S. Schütz, G. Guthausen, New insights into sodium alginate fouling of ceramic hollow fiber membranes by NMR imaging, AIChE Journal 62 (2016) 2459–2467.

[38] S. Chang, A. Yeo, A.G. Fane, M. Cholewa, Y. Ping, H. Moser, Observation of flow characteristics in a hollow fiber lumen using non-invasive X-ray microimaging (XMI), J. Membr. Sci. 304 (2007) 181–189.

[39] A. Yeo, P. Yang, A.G. Fane, T. White, H.O. Moser, Non-invasive observation of external and internal deposition during membrane filtration by X-ray microimaging (XMI), J. Membr. Sci. 250 (2005) 189–193.

[40] A.P. Mairal, A.R. Greenberg, W.B. Krantz, L.J. Bond, Real-time measurement of inorganic fouling of RO desalination membranes using ultrasonic time-domain reflectometry, J. Membr. Sci. 159 (1999) 185–196.

[41] J.X. Li, D.K. Hallbauer, R.D. Sanderson, Direct monitoring of membrane fouling and cleaning during ultrafiltration using a non-invasive ultrasonic technique, J. Membr. Sci. 215 (2003) 33–52.

[42] K.D. Cobry, Z. Yuan, J. Gilron, V.M. Bright, W.B. Krantz, A.R. Greenberg, Comprehensive experimental studies of early-stage membrane scaling during nanofiltration, Desalination 283 (2011) 40–51.

[43] J.X. Li, V.Y. Hallbquer-Zadorozhnaya, D.K. Hallbauer, R.D. Sanderson, Cake-layer deposition, growth, and compressibility during microfiltration measured and modeled using a noninvasive ultrasonic technique, Ind. Eng. Chem. Res. 41 (2002) 4106–4115.

[44] R.D. Sanderson, J.X. Li, D.K. Hallbauer, S.K. Sikder, Fourier wavelets from ultrasonic

spectra: a new approach for detecting the onset of fouling during microfiltration of paper mill effluent, Environ. Sci. Technol. 39 (2005) 7299–7305.

[45] X.C. Xu, J.X. Li, H.S. Li, Y. Cai, Y.H. Cao, B.Q. He, Y.Z. Zhang, Non-invasive monitoring of fouling in hollow fiber membrane via UTDR, J. Membr. Sci. 326 (2009) 103–110.

[46] X.C. Xu, J.X. Li, N.N. Xu, Y.L. Hou, J.B. Lin, Visualization of fouling and diffusion behaviors during hollow fiber microfiltration of oily wastewater by ultrasonic reflectometry and wavelet analysis, J. Membr. Sci. 341 (2009) 195–202.

[47] X.H. Li, J.X. Li, J. Wang, H.W. Zhang, Y.D. Pan, In situ investigation of fouling behavior in submerged hollow fiber membrane module under sub-critical flux operation via ultrasonic time domain reflectometry, J. Membr. Sci. 411–412 (2012) 137–145.

[48] X.H. Li, J.X. Li, J. Wang, H. Wang, B.Q. He, H.W. Zhang, Ultrasonic visualization of sub-critical flux fouling in the double-end submerged hollow fiber membrane module, J. Membr. Sci. 444 (2013) 394–401.

[49] X.H. Li, J.X. Li, J. Wang, H. Wang, Z.Y. Cui, B.Q. He, H.W. Zhang, Direct monitoring of sub-critical flux fouling in a horizontal double-end submerged hollow fiber membrane module using ultrasonic time domain reflectometry, J. Membr. Sci. 451 (2014) 226–233.

[50] A. Antony, T. Chilcott, H. Coster, G. Leslie, In situ structural and functional characterization of reverse osmosis membranes using electrical impedances pectroscopy, J. Membr. Sci. 425-426 (2013) 89–97.

[51] L. Gaedt, T.C. Chilcott, M. Chan, T. Nantawisarakul, A.G. Fane, H.G.L. Coster,

Electrical impedance spectroscopy characterization of conducting membranes II. Experimental, J. Membr. Sci. 195 (2002) 169–180.

[52] S. Bannwarth, M. Darestani, H. Coster, M. Wessling, Characterization of hollow fiber membranes by impedance spectroscopy, J. Membr. Sci. 473 (2015) 318–326.

[53] S. Bannwarth, T. Trieu, C. Oberschelp, M. Wessling, On-line monitoring of cake layer structure during fouling on porous membranes by in situ electrical impedance analysis, J. Membr. Sci. 503 (2016) 188–198.

[54] M.S. Chun, H.I. Cho, I.K. Song, Electrokinetic behavior of membrane zeta potential during the filtration of colloidal suspensions, Desalination 148 (2002) 363–367.

[55] J.H. Sung, M.S. Chun, H.J. Choi, On the behavior of electrokinetic streaming potential during protein filtration with fully and partially retentive nanopores, J. Colloid Interface Sci. 264 (2003) 195–202.

[56] Y. Lanteri, P. Fievet, S. Déon, P. Sauvade, W. Ballout, A. Szymczyk, Electrokinetic characterization of hollow fibers by streaming current, streaming potential and electric conductance, J. Membr. Sci. 411–412 (2012) 193–200.

[57] H. Jia, H.M. Zhang, J. Wang, H.W. Zhang, X.B. Zhang, Response of zeta potential to different types of local membrane fouling in dead-end membrane filtration with yeast suspension, RSC Adv. 5 (2015) 78738–78744.

[58] J. Wang, S.S. Yang, W.S. Guo, H.H. Ngo, H. Jia, J. Yang, H.W. Zhang, X.B. Zhang, Characterization of fouling layers for in-line coagulation membrane fouling by apparent zeta potential, RSC Adv. 5 (2015) 106087–106093.

[59] M.J. Clifton, N. Abidine, P. Aptel, V. Sanchez, Growth of the polarization layer in

ultrafiltration with hollow-fibre membranes, J. Membr. Sci. 3 (1984) 233–245.

[60] S.H. Yoon, S.H. Lee, I.T. Yeom, Experimental verification of pressure drop models in hollow fiber membrane, J. Membr. Sci. 310 (2008) 7–12.

[61] W.N. Lee, W.S. Cheong, K.M. Yeon, B.K. Hwang, C.H. Lee, Correlation between local TMP distribution and bio-cake porosity on the membrane in a submerged MBR, J. Membr. Sci. 332 (2009) 50–55.

[62] J. Wang, Z. Cui, H. Jia, H.W. Zhang, The effect of fiber length on non-uniform and hysteresis phenomenon in hollow fiber membrane backflushing, Desalination 337 (2014) 98–108.

[63] X.H. Li, J.X. Li, J. Wang, H. Wang, B.Q. He, H.W. Zhang, W.S. Guo, H.H. Ngo, Experimental investigation of local flux distribution and fouling behavior in double-end and dead-end submerged hollow fiber membrane modules, J. Membr. Sci. 453 (2014) 18–26.

[64] B.J. Pangrle, E.G. Walsh, S.C. Moore, D. DiBiasio, Investigation of fluid flow patterns in a hollow fibre module using magnetic resonance velocity imaging, Biotechnol. Tech. 3 (1989) 67–72.

[65] B.J. Pangrle, E.G. Walsh, S.C. Moore, D. DiBiasio, Magnetic resonance imaging of laminar flow in porous tube and shell systems, Chem. Eng. Sci. 47 (1992) 517–526.

[66] S. Yao, M. Costello, A.G. Fane, J.M. Pope, Non-invasive observation of flow profiles and polarization layers in hollow fibre membrane filtration modules using NMR micro-imaging, J. Membr. Sci. 99 (1995) 207–216.

[67] S. Laukemper-Ostendorf, H.D. Lemke, P. Blümler, B. Blümich, NMR imaging of flow

in hollow fiber hemodialyzers, J. Membr. Sci. 138 (1998) 287–295.

[68] P.A. Hardy, C.K. Poh, Z. Liao, W.R. Clark, D. Gao, The use of magnetic resonance imaging to measure the local ultrafiltration rate in hemodialyzers, J. Membr. Sci. 204 (2002) 195–205.

[69] T. Osuga, T. Obata, H. Ikehira, Detection of small degree of nonuniformity in dialysate flow in hollow fiber dialyzer using proton magnetic resonance imaging, J. Membr. Sci. 22 (2004) 417–420.

[70] C.K. Poh, P.A. Hardy, Z.J. Liao, Z. Huang, W.R. Clark, D. Gao, Effect of flow baffles on the dialyzsate flow distribution of hollow fiber hemodialyzers: a nonintrusive experimental study using MRI, J. Biomech. Eng. 125 (2003) 481–489.

[71] X. Yang, E.O. Fridjonsson, M.L. Johns, R. Wang, A.G. Fane, A non-invasive study of flow dynamics in membrane distillation hollow fiber modules using low-field nuclear magnetic resonance imaging (MRI), J. Membr. Sci. 241 (2004) 23–44.

[72] H.H. Bruun, Hot Wire Anemometry: Principles and Signal Analysis, Oxford University Press, 1995.

[73] J.S. Eow, B. Zhang, M. Ghadiri, Flow maldistribution and corner fluidization in non-uniform packed beds: pressure and velocity profiles, Powder Technol. 138 (2003) 169–188.

[74] A. Madec, PhD thesis, Influence dun ecoulement diphasique sur les performances de filtration dun procede a membranes immergees, Institut National des Sciences Appliquees, 2000.

[75] D. Meunier, S. Tardu, D. Tsamados, J. Boussey, Realization and simulation of wall

shear stress integrated sensors, Microelectron. J. 34 (2003) 1129–1136.

[76] P. Le-Clech, Z. Cao, P.Y. Wan, D.E. Wiley, A.G. Fane, The application of constant temperature anemometry to membrane processes, J. Membr. Sci. 284 (2006) 416–423.

[77] F. Wicaksana, A.G. Fane, A.W.K. Law, The use of constant temperature anemometry for permeate flow distribution measurement in a submerged hollow fibre system, J. Membr. Sci. 339 (2009) 195–203.

[78] Y. Sato, M. Mineshima, I. Ishimori, I. Kaneko, T. Akiba, S. Teraoka, Effect of hollow fiber length on solute removal and quantification of internal filtration rate by Doppler ultrasound, Int. J. Artif. Organs. 26 (2003) 129–134.

[79] M. Mineshima, I. Ishimori, R. Sakiyama, Validity of internal filtration enhanced hemodialysis as a new hemodiafiltration therapy, Blood Purif. 27 (2009) 33–37.

[80] M. Mineshima, Estimation of internal filtration flow rate in high-flux dialyzers by doppler ultrasonography, Contrib Nephrol. 168 (2011) 153–161.

[81] R. Sakiyama, I. Ishimori, T. Akiba, M. Mineshima, Effect of blood flow rate on internal filtration in a high-flux dialyzer with polysulfone membrane, J. Artif. Organs. 15 (2012) 266–271.

[82] G. Iorio, E. Drioli, B. Memoli, V.E. Andreucci, M. Salvatore, B. Alfano, Ultrafiltration processes in blood treatment, J. Membr. Sci. 18 (1984) 297–311.

[83] C. Ronco, A. Lupi, A. Brendolan, M. Feriani, C. Crepaldi, G. La Greca, Ultrafiltration and pressure profiles in continuous arterio-venous hemofiltration studied by computerized scintigraphic imaging, Int. J. Artif. Organs, 14(8) (1991) 457–462.

[84] C. Ronco, A. Brendolan, M. Feriani, M. Milan, P. Conz, A. Lupi, P. Berto, M. Brttini, G.

La Greca, A new scintigraphic method to characterize ultrafiltration in hollow fiber dialyzers, Kidney Int. 41 (1992) 1383–1393.

[85] M. Defossez, L. Ding, M. Jaffrin, M. Fauchet, Scintigraphic study of local flux and osmotic pressure distributions in ultrafiltration of blood and plasma, J. Colloid Interface Sci. 177 (1996) 179–191.

[86] C. Ronco, G. Orlandini, A. Brendolan, A. Lupi, G. Greca, Enhancement of convective transport by internal filtration in a modified experimental hemodialyzer Technical Note, Kidney Int. 54 (1998), 979–985.

[87] C. Legallais, E. Doré, L. Ploux, M. Fauchet, M.Y. Jaffrin, A scintigraphic study of LDL-cholesterol irreversible trapping in a plasma fractionation membrane, Chem. Eng. Sci. 53 (1998) 2623–2640.

[88] G.B. Fiore, G. Guadagni, A. Lupi, Z. Ricci, C. Ronco, A new semiempirical mathematical model for prediction of internal filtration in hollow fiber hemodialyzers, Blood Purif. 24 (2006) 555–568.

[89] A. Balducci, M. Grigioni, G. Querzoli, G.P. Romano, C. Daniele, G.D. Avenio, V. Barbaro, Investigation of the flow field downstream of an artificial heart valve by means of PIV and PTV, Exp. Fluids 36 (2004) 204–213.

[90] B. Balakumar, R. Adrian, Particle-image velocimetry measurement in the exhaust of a solid rocket motor, Exp. Fluids 36 (2004) 166–175.

[91] A.P.S. Yeo, A.W.K. Law, A.G. Fane, Factors affecting the performance of a submerged hollow fiber bundle, J. Membr. Sci. 280 (2006) 969–982.

[92] A.P.S. Yeo, A.W.K. Law, A.G. Fane, The relationship between performance of

submerged hollow fibers and bubble-induced phenomena examined by particle image velocimetry, J. Membr. Sci. 304 (2007) 125–137.

[93] L. Martinelli, C. Guigui, A. Line, Characterisation of hydrodynamics induced by air injection related to membrane fouling behaviour, Desalination 250 (2010) 587–591.

[94] M. Pourbozorg, T. Li, A.W.K. Law, Effect of turbulence on fouling control of submerged hollow fibre membrane filtration, Water Res. 99 (2016) 101–111.

[95] T. Li, A.W.K. Law, M. Cetin, A.G. Fane, Fouling control of submerged hollow fibre membranes by vibrations, J. Membr. Sci. 427 (2013) 230–239.

[96] X.F. Liu, Y. Wang, T.D. Waite, G. Leslie, Numerical simulation of bubble induced shear in membrane bioreactors: Effects of mixed liquor rheology and membrane configuration, Water Res. 75 (2015) 131–145.

[97] X.F. Liu, Y. Wang, T.D. Waite, G. Leslie, Numerical simulations of impact of membrane module design variables on aeration patterns in membrane bioreactors, J. Membr. Sci. 520 (2016) 201–213.

[98] G.H. An, J.B. Lin, J.X. Li, X.H. Li, X.Q. Jian, Non-invasive measurement of membrane scaling and cleaning in spiral-wound reverse osmosis modules by ultrasonic time-domain reflectometry with sound intensity calculation, Desalination 283 (2011) 3-9.

[99] S.T.V. Sim, W.B. Krantz, T.H. Chong, A.G. Fane, Online monitor for the reverse osmosis spiral wound module — Development of the canary cell, Desalination 368 (2015) 48–59.

Fig. 1. (a) NMR imaging configuration for the hollow fiber membrane [32] and (b) the evolution of cake layer formation [35].

Fig. 2. (a) Setup of the phase contrast imaging and tomography at the Singapore Synchrotron Light Source [38] and (b) XMI showing the progressive deposition of iron hydroxide on the lumen wall [39].

Fig. 3. Schematic diagram of UTDR measurement in a hollow fiber membrane module and the corresponding time-domain response after (a) 0 (start) and (b) 60 min of fouling operation [45].

Fig. 4. 2D color contour diagrams and 3D representations of wavelet magnitude transformed from ultrasonic signals detected after (a) 0 min, (b) 60 min and (c) 420 min of fouling operation [46].

Fig. 5. (a) Schematic diagram of the EIS measurement principle and (b) the bode plots of the impedance measurements [52].

Fig. 6. Schematic diagram of the experimental set-up for the tangential streaming potential measurement [56].

Fig. 7. Flux and zeta potential variations vs. filtration time at three different positions of the membrane module [57].

Fig. 8. (a) Schematic diagrams of experimental setup and (b) comparison of experimental and theoretical results in the case of deionized water [60].

Fig. 9. Schematic diagrams of (a) the experimental setup and (b) variations in the water level

during suction [61].

Fig. 10. Local flux distribution along the fiber in the dead-end and double-end submerged hollow fiber membrane modules [63].

Fig. 11. Schematics of (a) the experimental setup and (b) the flux distribution under different aerated conditions [77].

Fig. 12. Doppler shift of the ultrasound beam [80].

Table 1. Non-invasive techniques to monitor hollow fiber membrane fouling.

Method	Principle	Configuration	Resolution	Type of foulants	Technical feature	Limitation	Refs.
Direct observation technique	Observation of fouling layer using the microscope /video-camera system	Pressurized mode	0.5 μm	Yeast, sodium alginate, latex particles or submicron bacteria	Low cost and relative high resolution	Require transparent membrane and relative clear solution	[22-31]
Magnetic resonance imaging	The signal intensity is a function of properties of the specimen (eg. chemical environment and local diffusion coefficient)	Submerged/ pressurized modes	10 μm	Colloidal silica and sodium alginate	Simultaneous observation of permeate flow and fouling layer	Low spatial resolution and specific device	[32-37]

X-ray microimaging	The amplitude and phase of X-ray are related to the material characterizations (eg. density and light velocity in a medium)	Pressurized mode	1 μm	Ferric hydroxide	High resolution	Specific and expensive device	[38-39]
Ultrasonic time-domain reflectometry	Ultrasonic waves changes caused by the acoustic impedance difference between membrane and fouling layer	Submerged/ pressurized modes	0.5μm	BSA, yeast, kaolin, oil	Simultaneously achieve the thickness and physical properties of the fouling layer	Lack of knowledge on acoustic wave propagation	[40-49]
Electrical impedance spectroscopy	Change in conductive and capacitive properties at the interface of foulant/membrane	Pressurized mode	0.1μm	Ferric hydroxide	High resolution	Alteration of membrane structure and specific module	[50-53]
Streaming potential measurement	The electrokinetics interactions of membrane/foulant and foulant/fouling layer	Submerged/ pressurized modes	0.1μm	Yeast, latex particles, BSA	High resolution and low complexity of equipment	Specific foulants	[54-58]

Table 2. Comprehensive comparison of monitoring methods for local filtration

characterization.

Method	Principle	Specific Membrane or Module	Configuration	Technical feature	Limitation	Refs.
Experimental segmentation method	The filtrate compartment was divided into several sub-compartments to continuously measure flux	Homemade module	Submerged mode	Simple and low cost	Invasive and low resolution	[59-63]
Magnetic resonance imaging	The signal intensity is related to the local diffusion coefficient of liquid	Module diameter < 30 cm	Submerged/ pressurized modes	Non-invasive, monitor simultaneously permeate flow and fouling layer	Require specialist support	[64-71]
Constant Temperature Anemometry	Any changes in fluid velocity will alter the convective heat transfer coefficient thereby affecting sensor temperature	Homemade module	Submerged mode	High-frequency response and excellent sensitivity	Fragile and sensitive to environmental changes	[72-77]
Doppler Ultrasonography	The velocity of blood flow will affect the Doppler shift	–	Pressurized mode	Non-invasive and low complexity	Be only applied to dialyzer	[78-81]
Scintigraphic method	The change in marked molecule is related to the	Material transparent to gamma	Pressurized mode	Non-invasive and high resolution	Require specialist support	[82-88]

	variation in the velocity of blood flow	ray				
Particle image velocitmetry	The changes in the particle position in the sequence of images reveals the Lagrangian velocity distribution	Transparent test tank	Submerged mode	Non-invasive	Require specialist support and complex data processing	[89-97]

Highlights

- In-situ monitoring techniques for the hollow fiber membrane fouling are reviewed.
- In-situ monitoring approaches of local filtration properties are summarized.
- The relationship between local filtration and fouling behaviors is discussed.
- The application of in-situ techniques to commercial modules is a critical issue.

Fig. 1

(Li et al.)

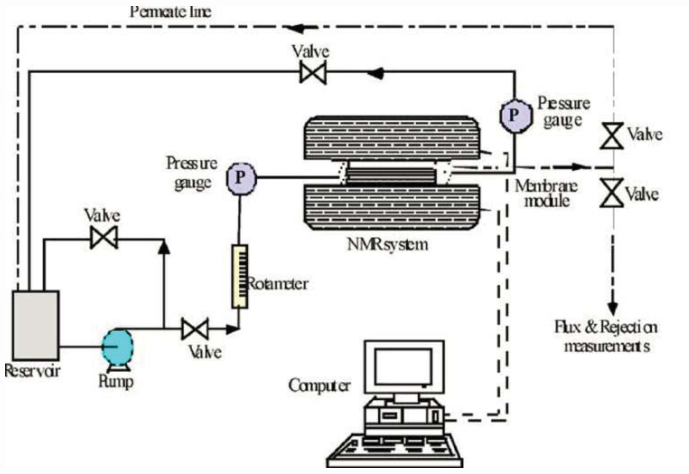

(a)

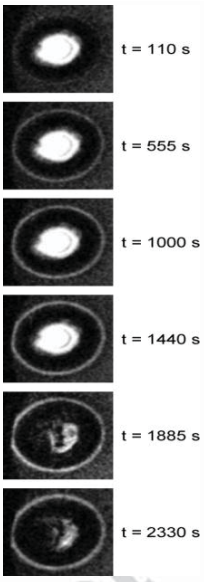

(b)

Fig. 2

(Li et al.)

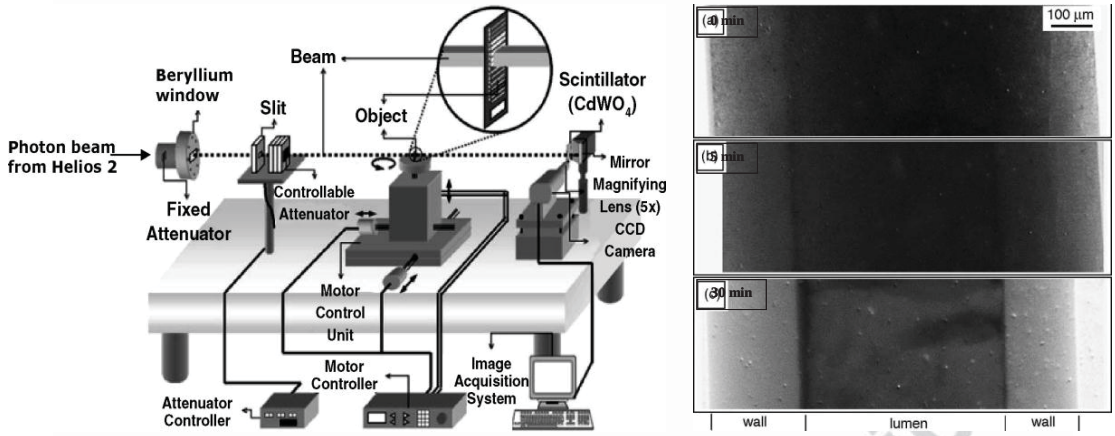

(a) **(b)**

Fig. 3

(Li et al.)

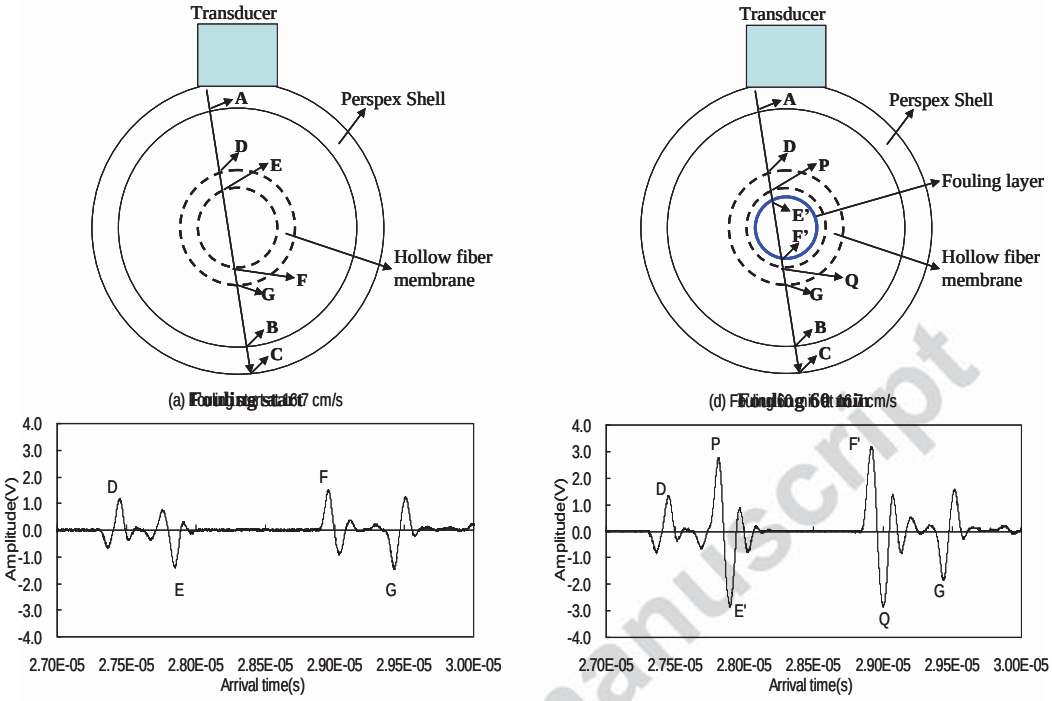

(a) **(b)**

Fig. 4

(Li et al.)

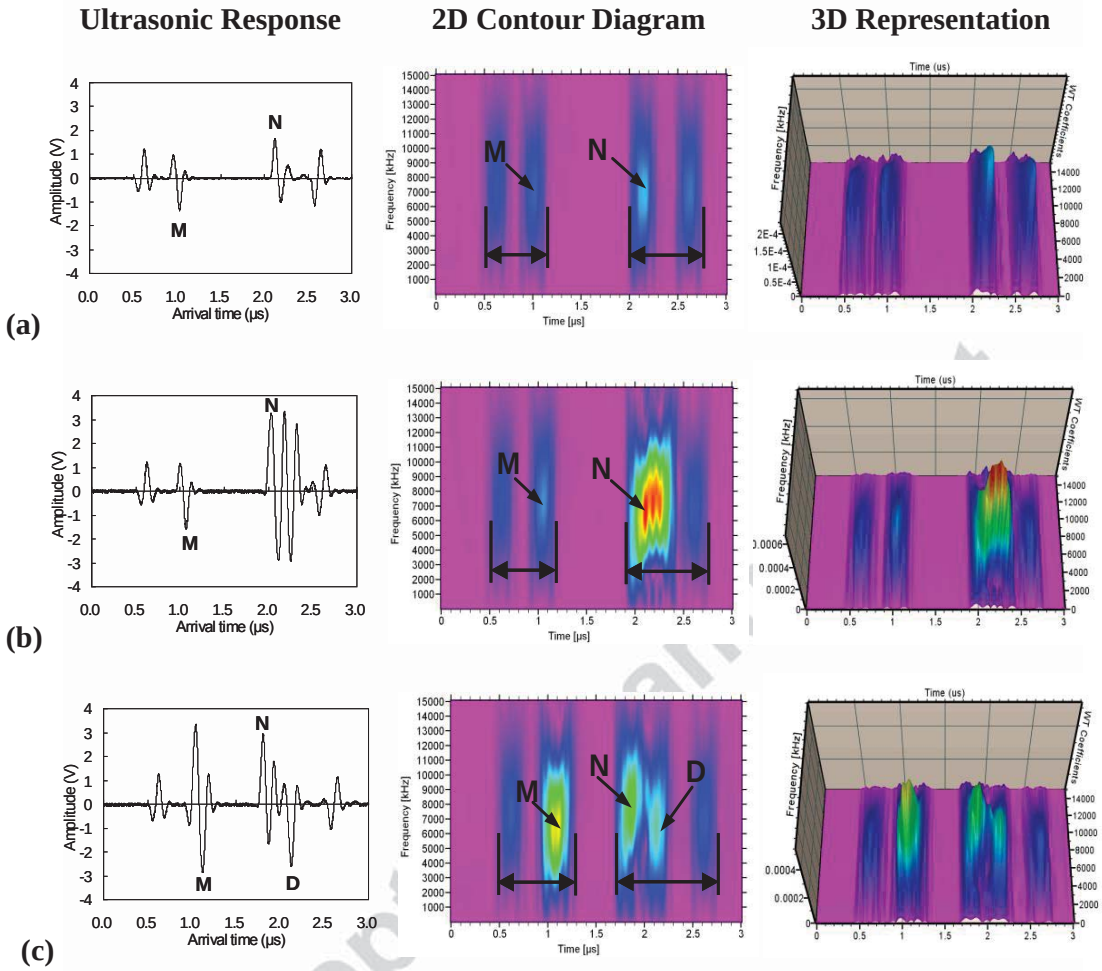

Fig. 5

(Li et al.)

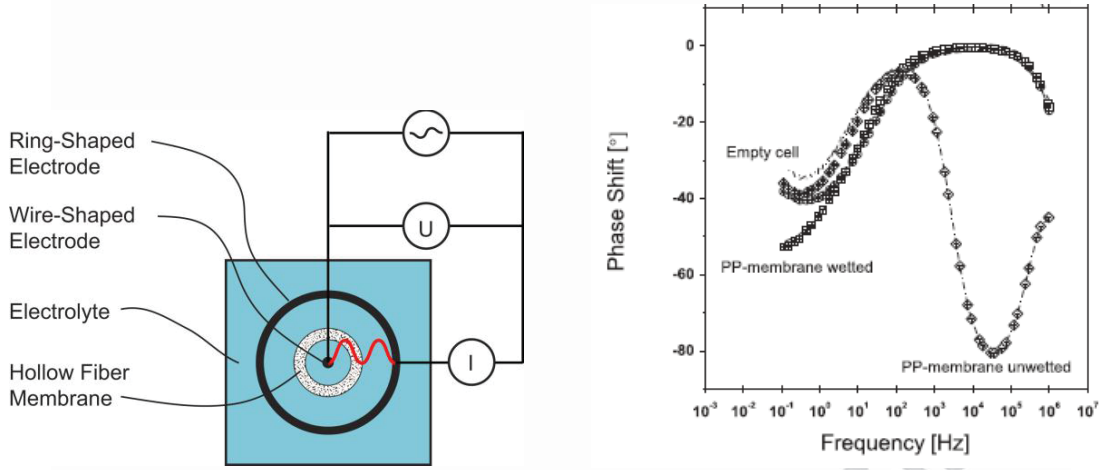

(a) **(b)**

Fig. 6

(Li et al.)

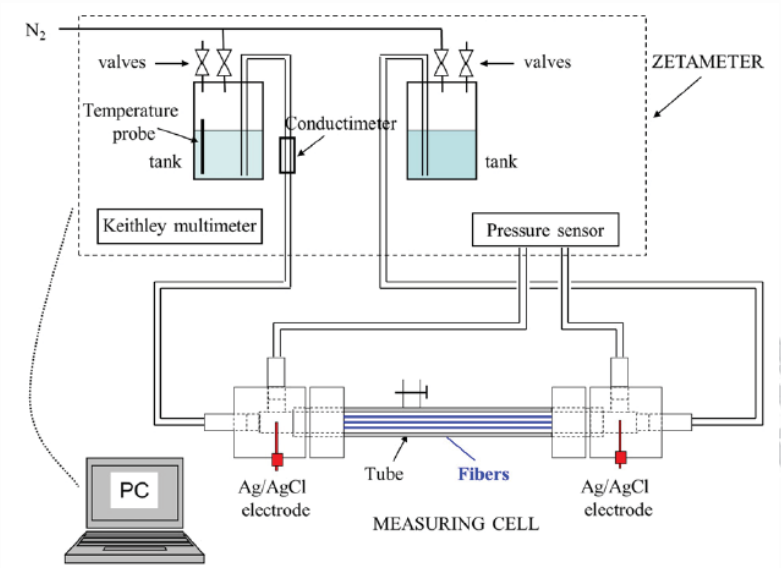

Fig. 7

(Li et al.)

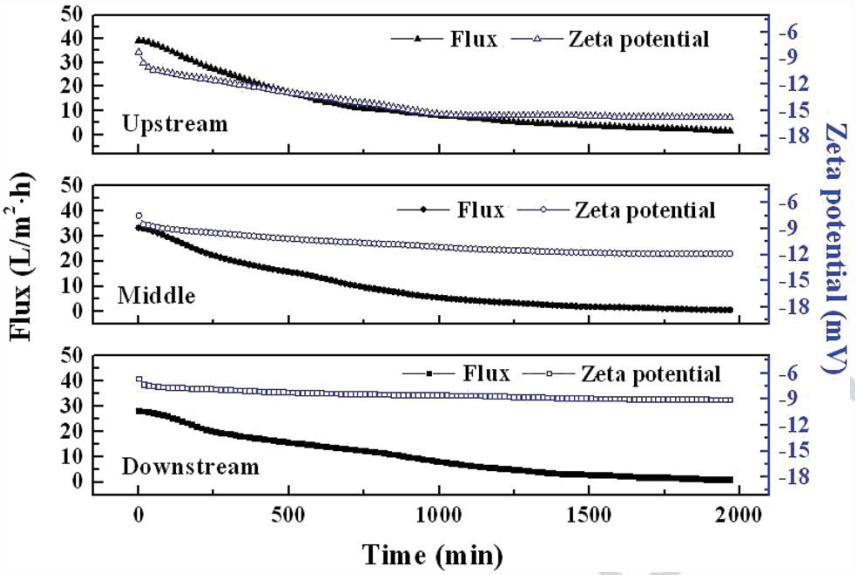

Fig. 8

(Li et al.)

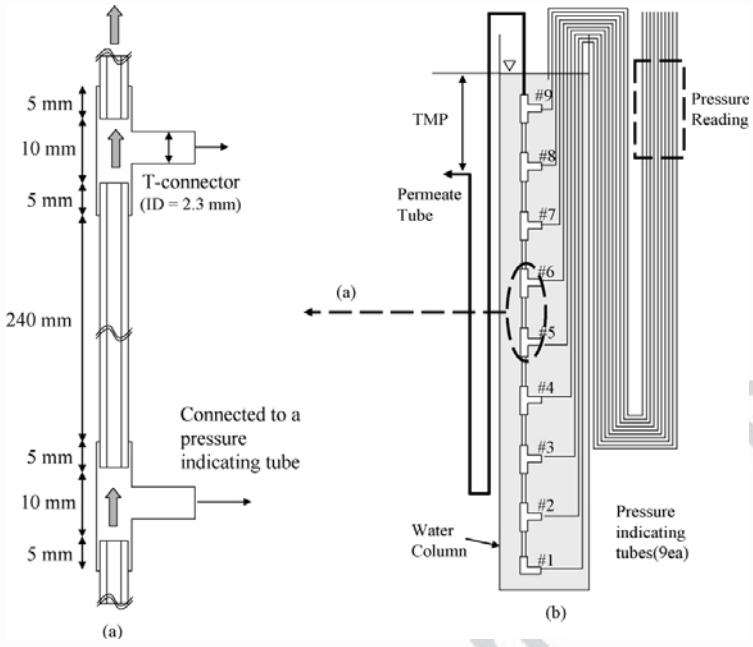

(a)

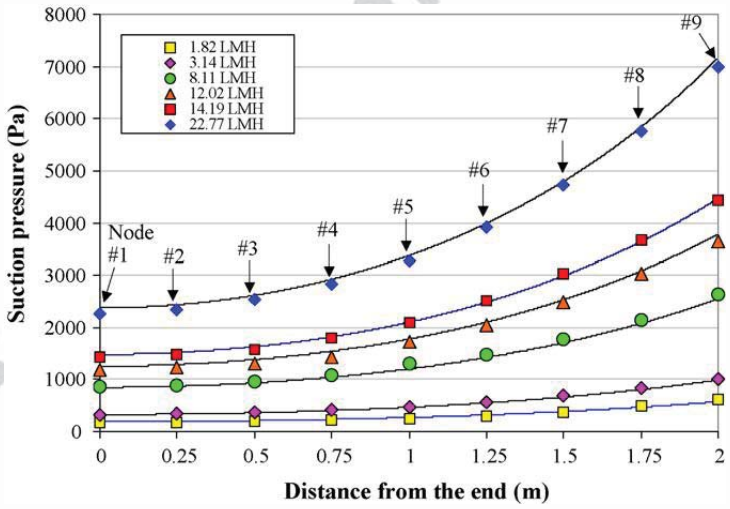

(b)

Fig. 9

(Li et al.)

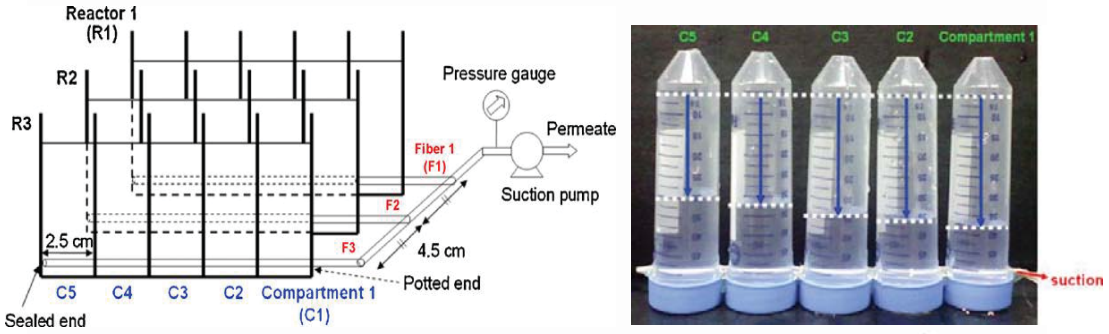

(a) **(b)**

Fig. 10

(Li et al.)

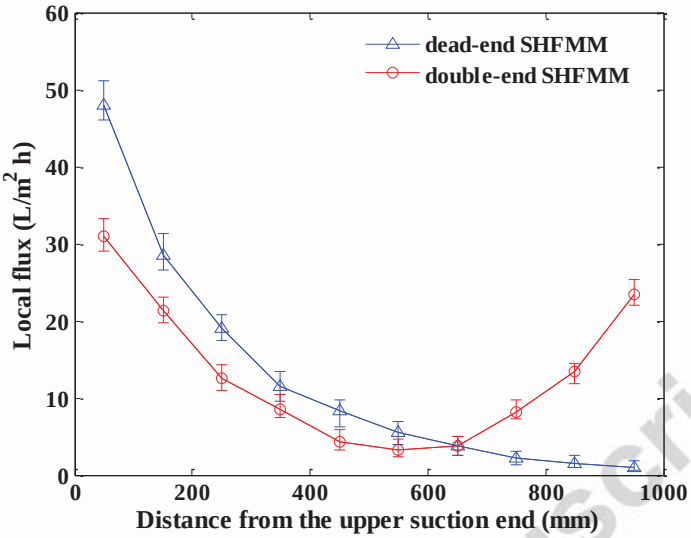

Fig. 11

(Li et al.)

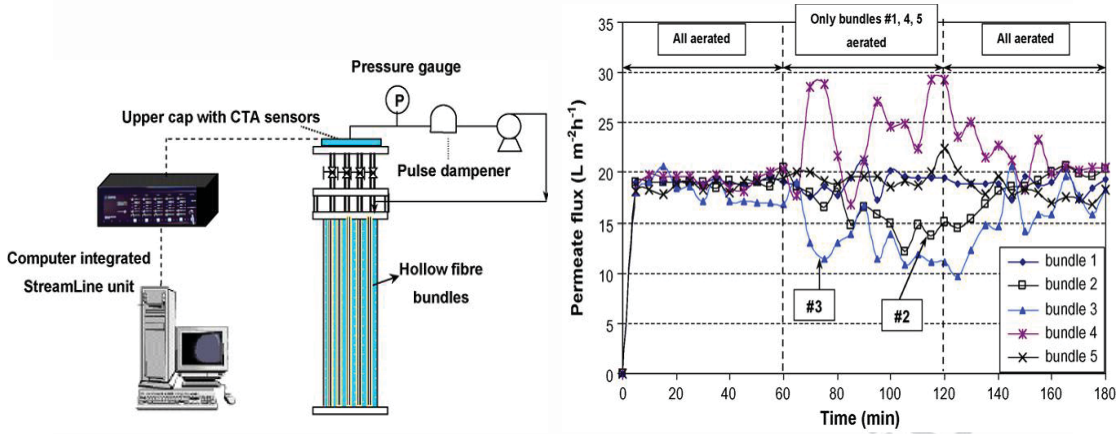

(a) **(b)**

Fig. 12

(Li et al.)